PROCEEDINGS OF SCIENCE

Cosmic ray variation caused by coronal mass ejections without direct impact on Earth

Y. Hayashi,[a,*] **C. Kato,**[a] **Y. Masuda,**[a] **M. Kozai,**[b] **R. Kataoka,**[c,d] **A. Kadokura,**[b,c,d] **S. Miyake**[e] **and K. Munakata**[a] **for the GMDN collaboration**

[a] *Physics Department Shinshu University, 3-1-1 Asahi, Matsumoto, Nagano 390-8621, Japan*

[b] *Polar Environment Data Science Center, Joint Support-Center for Data Science Research, Research Organization of Information and Systems, Tachikawa, Tokyo 190-0014, Japan*

[c] *National Institute of Polar Research, Tachikawa, Tokyo 190-8518, Japan*

[d] *Department of Polar Science, School of Multidisciplinary Sciences, The Graduate University for Advanced Studies, SOKENDAI, Tachikawa, Tokyo 190-8518, Japan*

[e] *National Institute of Technology (KOSEN), Ibaraki College,866 Nakane, Hitachinaka-shi, Ibaraki-ken 312-8508 Japan*

E-mail: 22ss205h@shinshu-u.ac.jp

By using both the neutron monitor data and the Global Muon Detector Network (GMDN) data recorded in global networks monitoring a wide rigidity range of primary cosmic rays, we analyze two long-lasting cosmic ray intensity decreases accompanied by strong anisotropy reported by Buatthaisong et al. [1]. The network data analysis enables to analyze cosmic ray density variations and anisotropy variations separately and accurately. This is not possible in the analysis of single neutron monitor data or muon detector data. From our preliminary analysis, we find periods with increasing and decreasing anisotropies during the long-lasting cosmic ray intensity decrease. We discuss the possible IMF structure which is responsible to the obtained cosmic ray decrease and anisotropy enhancement.

38th International Cosmic Ray Conference (ICRC2023)
26 July - 3 August, 2023
Nagoya, Japan

∗Speaker

PoS(ICRC2023)1267

1. Introduction

The galactic cosmic ray (GCR) flux decreases temporarily when coronal mass ejections (CMEs) and/or interplanetary (IP) shocks arrive at Earth. This is called the Forbush decrease (FD) which is often observed by the space-borne and ground-based detectors.

Buatthaisong et al. [1] reported long-lasting cosmic ray intensity decreases with strong anisotropy observed by the PSNM, which monitors the highest energy cosmic rays in the worldwide neutron monitor (NM) network, in January and July, 2012. We are observing cosmic ray variations with the Global Muon Detector Network (GMDN) composed of four ground-based multidirectional muon detectors (MDs). NMs have maximum responses to ~15 GV primary cosmic rays on average, while the GMDN has maximum response to ~65 GV cosmic rays. By analyzing NM and MD data observed by global networks, we can deduce the variations of cosmic ray density (or isotropic intensity) and anisotropy separately and accurately over a wide rigidity range.

In this paper, we analyze NM and GMDN data and deduce variations of cosmic ray density and anisotropy, each as a function of time and the rigidity of primary cosmic rays, by performing the best-fit analysis presented in Munakata et al. [2], and report preliminary results.

2. Data and analysis

2.1 Cosmic-ray data

Table1 lists characteristics of NMs and MDs used in this study. The analysis is performed using hourly count rates of 18 NMs and 60 directional channels of the GMDN, when there is no missing data. These data are available in websites (NMDB : https://www.nmdb.eu/data/, PSNM : http://www.thaispaceweather.com/, GMDN : http://cosray.shinshu-u.ac.jp/crest/DB/Public/main.php, see also [3]). The data of NMs are corrected for atmospheric pressure effect, while the GMDN data are corrected for atmospheric pressure and temperature effects. For the atmospheric temperature correction of MD data, we use the method developed by Mendonça et al. [4] and GDAS data available in the NOAA website (ftp://ftp.arl.noaa.gov/archives/gdas1/).

2.2 Analysis

In this study, we perform the best-fit analysis using the following model function for the count rate recorded in the j-th directional channel of the i-th detector at the universal time t,

$$I_{i,j}^{fit}(t) = I_{i,j}^{CG}(t) + \sum_{n=0}^{2}\sum_{m=0}^{n}\{\xi_c^{n,m}(c_{i,j}^{n,m}\cos m\omega t_i - s_{i,j}^{n,m}\sin m\omega t_i) + \xi_s^{n,m}(t)(s_{i,j}^{n,m}\cos m\omega t_i + c_{i,j}^{n,m}\sin m\omega t_i)\}, \quad (1)$$

where $\xi_c^{0,0}(t)$ is the cosmic ray density, $\xi_c^{n,m}(t)$ and $\xi_s^{n,m}(t)(1 \le n \le 2, 0 \le m \le n)$ are the components of cosmic ray anisotropy in the GEO coordinates, t_i is the local time at the i-th detector, $c_{i,j}^{n,m}$ and $s_{i,j}^{n,m}$ are the coupling coefficients, and $\omega = \pi/12$. In the GEO coordinate system, we set the x-axis to the anti-sunward direction in the equatorial plane, the z -axis to the geographical north perpendicular to the equatorial plane, and the y-axis completing the right-handed coordinate

system. $I_{i,j}^{CG}(t)$ indicates a term for correcting the contribution from the solar wind convection and the Compton-Getting anisotropy arising from Earth's revolution around Sun. When we calculate coupling coefficients, we assume power-law spectra for the rigidity dependences of $\xi_c^{n,m}(t)$ and $\xi_s^{n,m}(t)$, as

$$g_n(p,t) = (p/p_r)^{\gamma_n(t)}, \tag{2}$$

where $\gamma_n(t)$ is the power-law index and p_r is the reference rigidity which is set at 15 GV representing the average median primary rigidity P_m monitored by NMs and at 65 GV representing the average median primary rigidity P_m monitored by the GMDN, respectively. In our previous analysis of the

Table 1: Characteristics of NMs and MDs

name	P_c(GV)	P_m(GV)
18NMs		
APTY	0.7	15.0
ATHN	8.3	22.8
BKSN	5.6	16.7
CALM	7.0	20.4
FSMT	0.3	15.1
INVK	0.3	15.1
JNGU1	4.5	13.5
KERG	1.1	14.9
LMKS	3.8	13.5
MXCO	8.2	20.4
NAIN	0.3	15.1
OULU	0.8	14.9
PWNK	0.3	15.1
SOPO	0.1	11.3
TERA	0.0	14.8
THUL	0.3	15.0
TXBY	0.5	14.9
PSNM	16.7	34.6
60 MD directional channels		
Nagoya (17 directional channels)	8.0-12.6	58.4-106.9
Hobart (13 directional channels)	2.5-4.0	53.1-74.0
Kuwait (13 directional channels)	8.9-14.1	61.2-104.0
São Martinho (17 directional channels)	7.1-14.1	54.3-98.4

Note: P_C and P_m indicate the geomagnetic cut-off rigidity and the median rigidity of primary GCRs, respectively.

GMDN data alone [5], $\gamma_n(t)$ is treated as a constant, as $\gamma_0 = -1$, $\gamma_1 = 0$, while Munakata et al. [2] treated it as a free parameter. γ_0 is the power-law index of rigidity spectra of the density, while γ_1, γ_2 are indices of the first- and second-order anisotropy, respectively. The following equation is used to calculate the amplitude of the first-order anisotropy.

$$A = \sqrt{\sum_{m=0}^{1} \{\xi_c^{1,m}(t)^2 + \xi_s^{1,m}(t)^2\}}. \tag{3}$$

3. Results

Figure 1 displays the best-fit cosmic ray parameters (panels (c)-(f)) together with the solar wind parameters (panels (a)-(b)) during two periods in 2012 as indicated at the top of figures. As seen in panels (a)-(b), there are abrupt enhancements of the solar wind velocity and IMF magnitude during these two periods, indicating the arrival of the solar wind disturbances accompanied by the IP shocks. The strong enhancements are seen in the first half of the period in January-February, while those are seen almost over entire period in July. The IMF orientation in panel (b) also indicates the IMF sector polarity changing several times during these periods and the "toward" sector is seen around the middle of each period in between the surrounding "away" sectors.

Both the cosmic ray densities at 15 GV and 65 GV in panel (c) decrease following the strong enhancement(s) of the solar wind velocity and IMF magnitude and then gradually recover. As seen in panel (d), these density decreases are accompanied by strong enhancements of the anisotropy with the maximum amplitude reaching ~1% in both periods, while the power-law index γ_1 of the anisotropy fluctuates around the average of ~0.0. The GEO-longitude (~300°) of the anisotropy orientation in panel (f), after the subtraction of the solar wind convection (see Eq. (1)), is roughly consistent with the cosmic ray streaming from the anti-sunward direction along the IMF (~315°). It is also noted that γ_0 of the density decreases in panel (e) are larger -1.0 during the majority of the density decrease periods indicating that the spectrum is harder than that known in typical Forbush decreases.

Another notable feature of the event in January-February is that an "additional" density decrease is seen in panel (c) in a few days around 32 doy at 15 GV, but no such decrease seen at 65 GV, indicating the softer rigidity spectrum of this additional decrease as seen in γ_0 decreasing in panel (e). There is no significant IP shock to be responsible for this decrease seen in the solar wind data. It is also interesting to see that the anisotropy amplitude in panel (d) decreases during this additional decrease.

In panel (d), sometimes a significant 24-hour variation is seen in the amplitude of the first-order anisotropy (black curves). This is due to the spurious anisotropy arising from the "local effect" and is also reported from the analysis of NM network data (Belov et al. [6]). This problem is discussed at this conference in Munakata et al. [7].

4. Summary

We analyzed NM and MD data each observed in a global network in January-February and July in 2012 and deduced the cosmic ray density and anisotropy on hourly basis each as a function

of the rigidity of primary cosmic rays. We found the extended density decreases accompanied by strong enhancements of the anisotropy. The rigidity spectra of the density decreases are harder than that known in typical Forbush decreases, while the amplitude of the enhanced anisotropy is rigidity independent on average. The orientation of the anisotropy is roughly consistent with the cosmic ray streaming from the anti-sunward direction along the IMF. In our future work, we will elucidate physical mechanisms causing the extended cosmic ray density decreases accompanied by strong anisotropy.

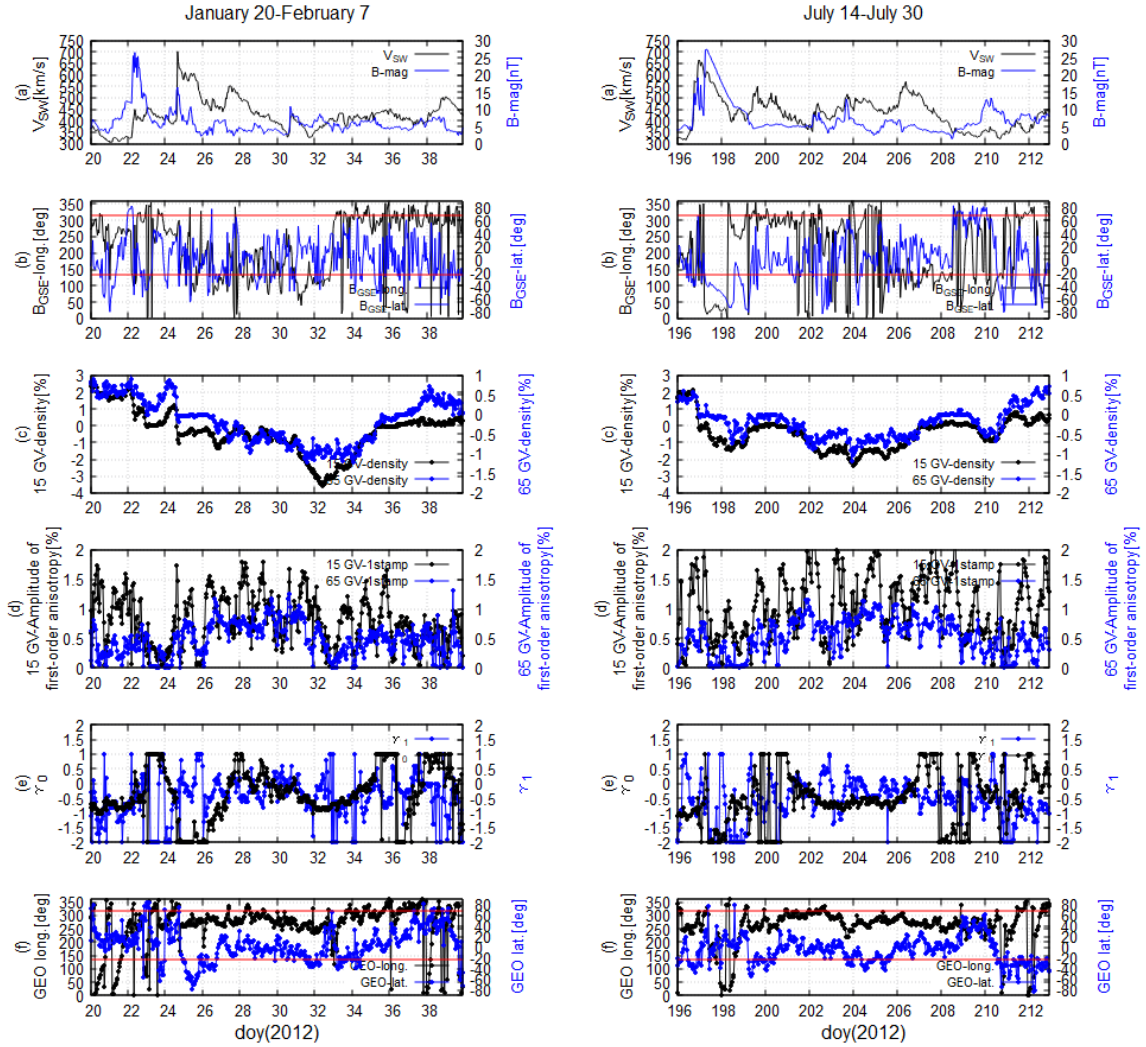

Figure 1: Best-fit cosmic ray parameters and solar wind parameters in January-February (left panels) and July (right panels). In all panels, black curves show parameters on the left vertical axis and blue curves show parameters on the right vertical axis, each as a function of time in the day of year. Panel (a) shows the solar wind speed and the magnetic field magnitude, (b) shows the GSE-longitude and latitude of the IMF orientation, (c) the cosmic-ray densities at 15 GV and 65 GV, (d) the amplitudes (A) of the first-order anisotropy at 15 GV and 65 GV, (e) the power-law indices of the density and the first-order anisotropy and (f) the GEO longitude and latitude of the orientation of the first-order anisotropy. Red horizontal lines in (b) and (f) indicate 135° and 315° representing the longitudes of the nominal Parker field orientations in the toward and away sectors, respectively.

5. Acknowledgement

This work is supported by the Institute for Space-Earth Environmental Research (ISEE), Nagoya University, the Institute for Cosmic Ray Research (ICRR), University of Tokyo, and the "Strategic Research Projects" grant from ROIS (Research Organization of Information and Systems) in Japan. The observations with the GMDN are supported by Nagoya University with the Nagoya muon detector, by INPE and UFSM with the São Martinho da Serra muon detector, by the Australian Antarctic Division with the Hobart muon detector, and by project SP01/09 of the Research Administration of Kuwait University with the Kuwait City muon detector. N. J. S. thanks the Brazilian Agency- CNPq for the fellowship under grant number 300886/2016-0. EE would like to thank Brazilian funding agencies for research grants FAPESP (2018/21657-1) and CNPq (pQ-301883/2019-0). M. Rockenbach thanks the Brazilian Agency - CNPq for the fellowship under grant number 306995/2021-2. ADL thanks CNPq for grant 309916/2018-6. PSNM maintenance was also supported by Achara Seripienlert and the National Astronomical Research Institute of Thailand. We acknowledge the NMDB database (http://www01.nmdb.eu/), founded under the European Union's FP7 program (contact no. 213007) for providing data. We also gratefully acknowledge the NOAA Air Resources Laboratory (ARL) for the provision of GDAS data, which are available at the READY website (http://www.ready.noaa.gov) and used in this paper. The OMNIWeb dataset of the solar wind and IMF parameters is provided by the Goddard Space Flight Center, NASA, USA.

References

[1] N. Buatthaisong et al, Astrophys. J., 21 (2022), https://doi.org/10.3847/1538-4357/ac96ea

[2] K.Munakata et al., Astrophys. J., 938, 30 (2022), https://doi.org/10.3847/1538-4357/ac91c5

[3] GMDN collaboration, Global Muon Detector Network (GMDN) data, http://hdl.handle.net/10091/0002001448

[4] R. R. S. Mendonça et al, Astrophys. J., 830 (2016), https://doi.org:10.3847/0004-637X/830/2/88

[5] W. Kihara et al., J. Space Weather, 19, 3 (2021), https://doi.org/10.1029/2020SW002531

[6] A. Belov et al., Solar Phys., 293 (2018), https://doi.org/10.1007/s11207-018-1277-6

[7] K. Munakata et al., Pos(ICRC2023)1228, (2023) in this conference

Full Authors List: GMDN Collaboration

K. Munakata[1], M. Kozai[2], C. Kato[1], Y. Hayashi[1], Y. Masuda[1], R. Kataoka[3,4], A. Kadokura[2,3,4], S. Miyake[5], K. Iwai[6] R. R. S. Mendonça[7], E. Echer[7], A. Dal Lago[7], M. Rockenbach[7], N. J. Schuch[8], J. V. Bageston[8], C. R. Braga[9], H. K. Al Jassar[10], M. M. Sharma[10], M. L. Duldig[11], J. E. Humble[11], I. Sabbah[12], P.-S. Mangeard[13], T. Kuwabara[13], and P. Evenson[13]

[1]Department of Physics, Shinshu University, Matsumoto, Nagano 390-8621, Japan. [2]Polar Environment Data Science Center, Joint Support-Center for Data Science Research, Research Organization of Information and Systems, Tachikawa, Tokyo 190-0014, Japan. [3]National Institute of Polar Research, Tachikawa, Tokyo 190-8518, Japan [4] Department of Polar Science, School of Multidisciplinary Sciences, The Graduate University for Advanced Studies, SOKENDAI, Tachikawa, Tokyo 190-8518, Japan [5] National Institute of Technology (KOSEN), Ibaraki College, 866 Nakane, Hitachinaka-shi, Ibaraki-ken 312-8508 Japan [6] Institute for Space-Earth Environmental Research, Nagoya University, Nagoya, Aichi 464-8601, Japan [7] National Institute for Space Research (INPE), 12227-010 São José dos Campos, Brazil [8] Southern Space Coordination, National Institute for Space Research, P.O. Box 5021-97110-970—Santa Maria, RS, Brazil [9] George Mason University, 4400 University Drive, Fairfax, VA 22030, USA [1]0 Physics Department, Kuwait University, P.O. Box 5969 Safat, 13060, Kuwait [1]1 School of Natural Sciences, University of Tasmania, Hobart, Tasmania 7001, Australia [1]2 Department of Laboratory Technology, College of Technological Studies, The Public Authority for Applied Education and Training, Shuwaikh, 72853, Kuwait. [13] Bartol Research Institute and Department of Physics and Astronomy, University of Delaware, 217 Sharp Laboratory, Newark, DE 19716, USA

PoS(ICRC2023)1267